Biosensors and Bioelectronics 130 (2019) 204–213

Contents lists available at ScienceDirect

Biosensors and Bioelectronics

journal homepage: www.elsevier.com/locate/bios

Dual-SERS biosensor for one-step detection of microRNAs in exosome and residual plasma of blood samples for diagnosing pancreatic cancer

Yuanfeng Pang[a], Chaoguang Wang[d], LuChun Lu[b], Chongwen Wang[b,*], Zhiwei Sun[a,*], Rui Xiao[c,*]

[a] Capital Medical University, Department of Toxicology, No. 10 Xitoutiao, You An Men, Beijing 100069, PR China
[b] College of Life Sciences, Anhui Agricultural University, Hefei 230036, PR China
[c] Beijing Institute of Radiation Medicine, Beijing Key Laboratory of New Molecular Diagnosis Techniques for Infectious Dedication, 27 Taiping Road, 100850 Beijing, PR China
[d] College of Intelligence Science and Technology, National University of Defense Technology, Changsha, Hunan 410073, PR China

ARTICLE INFO

Keywords:
Dual-SERS
Pancreatic cancer
Exosomal microRNA
Recycling signal amplification
One-step

ABSTRACT

MicroRNAs have been proved to be the biomarker for early detection of pancreatic cancer and the precisely quantitation of the MicroRNA-10b in the blood samples even can distinguish pancreatic cancer from chronic pancreatitis (CP) and normal controls (NC). In this study, we developed a DSN-assisted dual-SERS biosensor for microRNA-10b in exosome and residual plasma of blood samples detection based on the Fe_3O_4 @Ag-DNA-Au@Ag@DTNB (SERS tag) conjugates. In presence of target microRNA, it can hybridized with the complementary DNA probes. DSN enzyme was then added to selectively cleaves the DNA probe of the DNA/microRNA duplex, SERS tags can be released from the Fe_3O_4@Ag and SERS intensity quenching can be triggered, the released microRNA can enter the cycle to decluster other DNA and SERS tags. Due to the dual-SERS enhancement of the Fe_3O_4@Ag-SERS tag conjugates and the recycling signal amplification, a detection limit of 1 aM with single-base recognition can be performed by one step. The target microRNA in plasma-derived exosome and residual supernatant plasma of blood samples from pancreatic ductal adenocarcinoma (PDAC), chronic pancreatitis (CP) and normal controls (NC) were directly quantified and significant SERS signal distinction can be found among them. The precise quantitation, one-step and one-pot operation can ensure this assay a promising future for point-of-care cancer diagnosis technology.

1. Introduction

Pancreatic ductal adenocarcinoma (PDAC) is a deadly malignancy characterized by an abundant stroma, marked resistance to chemotherapy and radiotherapy, and advanced stage at clinical presentation precluding resection in 80% of patients (Ellis et al., 2009; Hidalgo, 2010). Since it exhibits no obvious early symptoms, patients often miss the best time for treatment. Consequently, the 5-year survival rate is only 9% (Siegel et al., 2016). Early detection and diagnosis is crucial for improving the therapeutic effect and the prognosis of the patients with pancreatic cancer. Traditional biomarkers such as carcinoembryonic antigen (CEA) and cancer antigen 19-9 (CA19-9) have improved the diagnostic accuracy of pancreatic cancer (Kim et al., 2017), but their specificity for pancreatic cancer is low because of high CA19-9 expression in benign pancreatic diseases and increased CEA expression in colorectal cancer (Datta and Vollmer, 2014; Goonetilleke and Siriwardena, 2007). As these biomarkers are not specific and sensitive enough to diagnose pancreatic carcinoma at early stages, it was valuable to discover specific biomarkers for early diagnosis of pancreatic carcinoma. MicroRNAs was a family of small non-coding RNA molecules (~22 nucleotides) which play a critical role in the post-transcriptional regulation of gene expression in the pathogenesis of many chronic diseases including cancer (Iorio and Croce, 2009). It has been found that microRNA expression patterns are altered in almost all cancer types suggesting that monitoring the expression of microRNAs may serve as reliable cancer biomarkers (Lee and Dutta, 2009; Wittmann and Jäck, 2010). For instance, it has been reported that the high expression level of microRNA-21, microRNA-155, microRNA-196a and miRcroNA-210 can be found in the serum of pancreatic carcinoma (Zeng et al., 2017). Recent studies have shown that microRNAs were key component of exosomal cargo and exosome delivered tumor microRNAs have been implicated in tumor progression via modulation of the microenvironment, angiogenesis, immune evasion, as well as metastasis (Thind et al., 2016). Moreover, compared with the free

* Corresponding authors.
E-mail addresses: yuanfengpang@163.com (Y. Pang), wangchaoguang@nudt.edu.cn (C. Wang), 571128828@qq.com (L. Lu), wangchongwen1987@126.com (C. Wang), 108243498@qq.com (Z. Sun), Ruixiao203@sina.com (R. Xiao).

https://doi.org/10.1016/j.bios.2019.01.039
Received 6 November 2018; Received in revised form 7 January 2019; Accepted 20 January 2019
Available online 25 January 2019
0956-5663/ © 2019 Elsevier B.V. All rights reserved.

microRNA in the serum, exosomal microRNAs are generally protected from degradation by RNase and more stable in the peripheral blood (Yoga and Yasunaga, 2011). Therefore, exosomal microRNAs represent ideal biomarkers for cancer diagnosis at the early stage (Ma et al., 2018). Numerous methods have been developed to detect exosomal microRNAs, such as microarrays (Fang et al., 2006) and quantitative reverse transcription polymerase chain reaction (qRT-PCR) (Li et al., 2009). However, the complicated manipulation, radioactive labeling steps and invalid internal controls disturbing plus the intrinsic properties of microRNAs, including short length, low abundance and high sequence similarity in biofluids, make the accurate detection of microRNA a real challenge (Dong et al., 2014). Other analytical techniques such as fluorescence-based assays (Xiao et al., 2018; Qu et al., 2018; Boriachek et al., 2018) and electrochemical (Ge et al., 2014; Ghazizadeh et al., 2018) have also been used to quantify the microRNAs. Although these strategies have made remarkable contributions to microRNA detection, the possibility of practical application in biofluid can also been restricted. For example, fluorescence-based assays often suffered of complicated manipulation and constituents species interfering of biological environment, which were readily perturbed by numerous experimental conditions such as thermodynamic fluctuations and dye photobleaching (Yang et al., 2015). Electrochemical platforms were susceptible by the high level of non-specific binding of biomolecules to the electrode surfaces and signal amplification strategies based on redox reporters sometimes lead to a loss of the dynamic range (Zhu et al., 2015; Qavi et al., 2010).

Surface-enhanced Raman spectroscopy (SERS) offers unique "signature" spectral profiles with very narrow peaks for individual analytes, thus providing the ability to detect multiple analytes due to the combination of molecular fingerprint specificity and single-molecule sensitivity (Li et al., 2013). Recently, SERS biosensor for microRNA detection has been pay attention as its advantages such as high sensitivity, fast, low cost, low background noise and anti-interference in diverse environments. Many SERS biosensors have been reported both based on capture probes/microRNA/signal probes "sandwich structure" (Qi et al., 2017; Zhou et al., 2017; Guo et al., 2018) or signal probes/microRNA "competitive hybridization with capture probes" especially with duplex-specific nuclease (DSN) assisting (Yang et al., 2018; He et al., 2017; Wu et al., 2018). Although these methods have shown good performance for microRNA detection even in human serum samples, the multiple reaction steps with multiple washing and hybridization will be time-consuming and each step will affect the accuracy of the whole method. Moreover, the sensitivity by these methods is limited to fM, which cannot compared with some electrochemical microRNA sensors with LOD of aM (Ghazizadeh et al., 2018).

To overcome these drawbacks, based on our previous Fe_3O_4@Ag based microRNA SERS biosensor (Pang et al., 2016), we proposed a one-step and one-pot assay for microRNAs detection based on DSN assisted dual-SERS biosensor. In this work, Fe_3O_4@Ag MNPs were synthesized both as capture and SERS substrate, Au core@Ag shell@Raman reporter (DTNB) nanostructures were synthesized as SERS tags. The Fe_3O_4@Ag-SERS tags assembles were formed through the DNA probes linking. Therefore, intense Raman signal can be induced by the "hot spots" between of the Au@Ag and Ag shell of Fe_3O_4@Ag substrate especially after magnetic concentration. As it has been reported that hydrolytic enzyme such as exonuclease III (Qu et al., 2017) or DSN (Ma et al., 2018) also have perfect performance for hydrolysis of DNA modified on the nanoparticles, here, we chose DSN for target microRNA recognition and cyclic signal amplification to improve the sensitivity. There are two main characteristic for our assay compared with previous SERS microRNA biosensors: first, the detection can be finished by one-step and one-pot without multiple washing and hybridization steps which was advantaged for clinic diagnosis. Second, due to the dual-SERS enhancement and DSN assisted recycle signal amplification, the detection limit of 1 aM with single-base recognition can be achieved, which was at least 100-fold lower than those of other methods using the SERS platform for microRNA detection as mentioned in the result and discussion section. More recently, Ma (Ma et al., 2018) has reported a SERS biosensor for exosomal microRNA detection by using Au@R6G@AgAu as SERS tag and silicon microbead as separating substrate with a LOD of 5 fM. For our assay, the Fe_3O_4@Ag substrate was more excellent not only for fast and simple separating performance through external magnetic field, but also to be used as LSPR substrate for dual-SERS enhancement of the Raman signal. To demonstrate the performance, we applied the SERS assay for microRNA-10b of biological fluids quantitation since it has been reported that microRNA-10b levels were significantly higher in plasma and exosomes from pancreatic ductal adenocarcinoma (PDAC) patients when compared with patients with chronic pancreatitis (CP) or normal controls (NC) (Joshi et al., 2015). Therefore, microRNA-10b can be expected as biomarker to distinguish PDAC from CP and health people. Combined with ultra-high sensitivity and selectivity, slight difference of the microRNA-10b levels both in the exosome and plasma samples of patients can be discovered to distinguish PDAC and CP. The one-step and one-pot operational process without any PCR amplification also make our biosensor a point-of-care tool for clinic diagnosis.

2. Experiment

2.1. Chemicals and reagents

Polyvinylpyrrolidone (PVP, MW 40 K), polyethyleneimine (PEI), ethanolamine, 5,5-dithiobis-(2-nitrobenzoic acid) (DTNB), 11-mercaptoundecanoic acid (MUA) and N-(3-dimethylaminopropyl)-N′-ethylcarbodiimide hydrochloride (EDC), DSN enzyme and reaction buffer (50 mM Tris-HCl, pH 8.0, 5 mM $MgCl_2$, and 1 mM DTT) were obtained from Sigma-Aldrich (USA). Ferric chloride ($FeCl_3{\cdot}6H_2O$),chloroauric acid tetrahydrate ($HAuCl_4{\cdot}4H_2O$), Silver nitrate ($AgNO_3$), ascorbic acid (AA), hexadecyltrimethylammonium bromide (CTAB), ethanolamine, MES(10 mM, pH 6.0), PBS(10 mM, pH 7.4),formaldehyde and streptavidin were purchased from Sinopharm Chemical Reagent Co. (Shanghai). The DNA oligonucleotides probe, with an amino-modified 5′ end and a modification of 3′ end by biotin, the microRNA-10b and microRNA-10a were synthesized by Sangon Biotech (Shanghai, China), the sequences were shown in Table S1. TRIzol RNA kit was purchased from Life Technologies (USA), RNase-free sterile water was used to prepare the buffer solutions. Healthy or patient serum samples were providing by the PLA 301 hospital with the empowerment of the patients.

2.2. Apparatus

UV–vis spectra was detected by on a Shimadzu 2600 spectrometer (Shimadzu, Japan). The surface morphology was characterized by scanning electron microscopy (SEM) (JEOL JSM-7001F, Japan), Energy-dispersive X-ray (EDX) spectra and high-resolution transmission electron microscopy (HRTEM) images were obtained via a JEOL JEM-2010F microscope at an accelerating voltage of 200 kV. Dynamic light scattering (DLS) data was detected by a Zetasizer Nano ZS (NANO-ZS 90, Malvern, UK). All SERS spectra were measured using a portable Raman system B&W Tek, i-Raman Plus BWS465–785H spectrometer. Samples were excited by a 785 nm laser with a power of 25 mW and a total acquisition time of 20 s for each SERS spectrum.

2.3. Preparation of streptavidin-modified Au@Ag@DTNB SERS tags and Fe_3O_4@Ag substrate

Firstly, Au NPs with a diameter of 30 ± 3 nm were synthesized according to the reported literature (Zhang et al., 2018). Briefly, 1% (w/v) $HAuCl_4$ and 1% trisodium citrate solution was mixed and boiled under stirring (100 °C) about 15 min, cooled the solution to thermally equilibrate to room temperature, the Au NPs with a diameter about

30 nm can be obtained. Encapsulation an outer Ag shell to the Au NPs was achieved following a previously reported method with some modifications (Wang et al., 2015a, 2015b). In brief, CTAB was dissolved in AuNP solution through sonication, freshly prepared AA (0.1 M) and silver nitrate solution (0.01 M) was added to the solution with a magnetic stirrer (700 rpm, 29 °C). Finally, NaOH solution (0.1 M) was added to elevate the pH to above 10 to initiate the Ag ion reduction reaction. After the color change was complete, the solution was centrifuged twice at 7500 rpm for 6 min to remove the excess reagents and redispersed in deionized water. Finally, 100 μL of freshly prepared DTNB solution (10 mM) was added to combine with the as-prepared Au@Ag NPs solution through Ag-SH covalent bonds. After incubated for 2 h and centrifuged at 7500 rpm for 6 min to remove the excess DTNB, the precipitate was resuspended in 1 mL of MES buffer (10 mM, pH 6.0). Finally, streptavidin was conjugated to the SERS tags as follows. First, 1 mL of Au@Ag@DTNB was reacted with 20 μL of EDC (5 mg/mL) for 20 min under vigorous shaking to activate the carboxyl of DTNB, then, 10 μL of streptavidin (1 mg/mL) was added, the streptavidin can conjugate with the DTNB through amino-carboxyl condensation. After shaking vigorously for 2 h, unreacted carboxyl of the SERS tags were blocked with 2% BSA for 1 h. The streptavidin-SERS tags were purified through two rounds of centrifugation (5800 rpm, 7 min) and then resuspended in 1 mL of PBS buffer (10 mM, pH 7.4) at 4 °C until use.

The high-performance Fe_3O_4@Ag MNPs were synthesized via a PEI-mediated seed growth method reported by us previously (Wang et al., 2015a, 2015b). Briefly, the Fe_3O_4@PEI nanoparticles were synthesized through a PEI self-assembly; Then, PEI-modified Fe_3O_4 was mixed with colloidal Au NPs (3 nm) and sonicated for 1 h to form Fe_3O_4@PEI-Au NPs. Finally, Fe_3O_4@PEI-Au NPs were dispersed in 100 mL of silver nitrate aqueous solution containing PVP (0.2 wt%), 100 μL of formaldehyde (37%) and 200 μL of ammonia solution (25%) for Fe_3O_4@Ag core-shell microspheres.

2.4. Fe_3O_4@Ag-DNA probe-SERS tag conjugation

The DNA probe (amine modified on 5′ and biotin modified on 3′) was immobilized on the surface of Fe_3O_4 @Ag as follow: Firstly, the preparative Fe_3O_4@Ag (1 mM) were sonicated in a MUA ethanol solution (20 mM) for 2 h to get surface carboxylation, secondly, 5 mL of EDC (5 mg/mL) was added to activate the carboxyl under vigorous shaking for 20 min. Finally, 5 mL of the capture DNA probes (1 μM) was added and shaken vigorously for 2 h and then blocked the unreacted carboxyl with 5% ethanolamine for 0.5 h. The streptavidin-modified SERS tag is conjugated onto Fe_3O_4@Ag-DNA probe by biotin-avidin interaction. Briefly, streptavidin-SERS tags (1 mL, 300 nM) were added to biotin-DNA-Fe_3O_4@Ag solution (1 mL, 50 nM) and incubated at room temperature for 1 h. Then, free SERS tags were removed by magnetic centrifugation. The Fe_3O_4@Ag-DNA probe-SERS tags conjugation were washed and then re-suspended in 2 mL of PBS buffer (10 mM, pH 7.4) at 4 °C until use. The synthetic process was shown in the Scheme 1.

2.5. Optimization of experiment conditions

Firstly, we studied the effect of temperature of DSN enzyme reaction. Under the same concentration of target microRNA (1 pM of microRNA-10b), DSN enzyme (0.5 U DSN, 2 μL of 1 × DSN master buffer), Fe_3O_4@Ag-SERS tags (100 nM, in PBS buffer) with the reaction time 60 min, different temperatures (30, 35, 40, 45, 50, 55 °C) were used to carry out the experiments, the SERS intensity of different tests was reordered (three replicate tests of different samples at each temperature). Secondly, we optimized the concentration of DSN enzyme ranging from 0.05 to 0.3 U with three replicates of each sample for each DSN concentration; finally, we optimized the reaction time with 20, 30, 40, 45, 50, 55 min, while each reaction time had three replicate tests of each sample. All of the reaction was performed in the same other conditions.

2.6. Cell culture, isolation of exosomes and exosomal RNA

PDCA patient-derived cancer cell lines (PANC-01), healthy pancreatic cells (HPDE6-C7) and human healthy breast cell line (MCF-10) and breast cancer cell line (MCF-7) were obtained from the American Type Culture Collection (Manassas, VA). Cell lines were cultured in RPMI-1640. Cell culture media were supplemented with 10% exosome depleted fetal bovine serum and 1% penicillin/streptomycin. The cells were maintained in a humidified incubator containing 5% CO_2 at 37 °C. The conditioned medium was collected after 60 h and centrifuged at 2000r for 30 min to eliminate the contaminants. Exosomes were isolated using the total exosome isolation reagent (Life Technologies,USA) following the manufacturer's instructions. The RNA was extracted from exosomes using the TRIzol RNA kit (Life Technologies,USA) following the manufacturer's instructions. The detail information can be seen in the reference (Boriachek et al., 2018).

2.7. Quantification of exosomal microRNA derived from cancer cell lines and microRNA in exosome and residual plasma of clinical blood samples

To determine the sensitivity of the assay, quantitative detection of microRNA-10b spiked in 10 μL buffer (0.25 U DSN enzyme with 1 × DSN master buffer) under the optimized conditions (45 °C and 50 min) was performed by our SERS assay by incubated with 30 μL Fe_3O_4@Ag-SERS tags (100 nM in PBS), after reaction, the residual was washed by deionized water and magnetic concentration for SERS spectra detection. To further demonstrate the applicability of this method in more complicated biological systems, microRNA spiked in plasma samples and microRNA of the total exosomal RNA isolated from the 4 cultured human cell lines were performed by the same process. Finally, for the clinic detection, blood samples were obtained from 5 PDAC patients who underwent resection for the cancer, 5 CP patients and 5 healthy controls. The samples were processed as the previous report (Joshi et al., 2015) primarily, samples were centrifuged twice at 10,000 rpm (4 °C, 30 min) and 100,000 rpm (4 °C, 30 min) respectively, then the supernatant was removed to a new tube for analysis the cyclic microRNA in the plasma, the precipitate was the washed with 1 × PBS and ultracentrifugedrepeatedly, the RNA was extracted from exosomes using the TRIzol RNA kit (Life Technologies, USA) following the manufacturer's instructions. Then, the target microRNA of the plasma and of the extracted RNA solutions were detected respectively as follow: 30 μL Fe_3O_4@Ag-DNA probe-SERS tags (100 nM) in PBS buffer (1 mM, pH 7.4) was incubated with RNA solution to capture the microRNA-10b for 1 h with gentle shaking at 37 °C. Then the complexes were incubated with 10 μL buffer (0.25 U DSN enzyme with 1 × DSN master buffer,0.5 U μL^{-1} RNase inhibitor) under the optimized conditions (45 °C and 50 min). After reaction, the residual complexes were washed and magnetic separated from the solution, then concentrated under the Raman laser through a magnet for SERS detection. SERS signal intensities at 1332 cm^{-1} using excitation laser wavelength of 785 nm and 20 s acquisition time was used for the sensitivity detection.

3. Results and discussion

3.1. Principle of the microRNA SERS detection based on DSN-assisted target recycling signal amplification

The synthesis process of the Fe_3O_4@Ag-DNA and SERS tags was illustrated in the Scheme 1a. The detection principle was shown in Scheme 1b. In the absent of microRNA, Fe_3O_4@Ag-DNA-SERS tags core-satellite assemblies can induce intense Raman signals as the dual-SERS enhancement of the combination of Au@Ag of SERS tag and Ag shell of Fe_3O_4@Ag especially after magnetic concentration,which can increase the electromagnetic hot spots further. In the presence of target

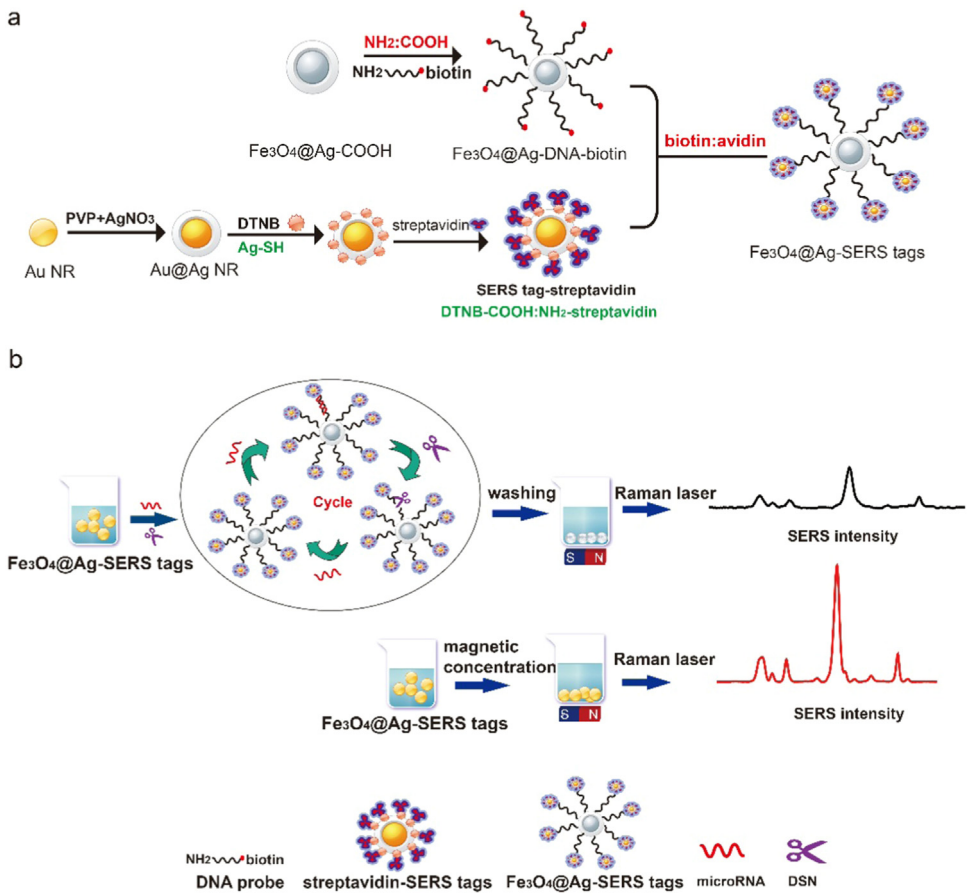

Scheme 1. (a) The synthesis process of Fe_3O_4@Ag-SERS tags (b) DSN-assisted SERS detection of microRNA.

microRNA, the DNA probe can hybridize with the microRNA. After incubation with DSN, it selectively cleaves the DNA of DNA/microRNA duplexes, therefore SERS tag can be separated from Fe_3O_4@Ag substrate to induce SERS signal quenching, the liberated microRNA can bind with additional DNA. It has been reported that one microRNA can cleave thousands of DNA probes (Yin et al., 2012) so that significant signal amplification can be expected. After the enzyme reaction, the residual assembles were magnetic separated and concentrated under the laser for Raman detection and the SERS signal decreasing was only correlated to the original concentration of microRNA. Moreover, as the specificity capability of DSN to discriminate between perfectly and no perfectly matched with one mismatch in DNA-DNA duplex (at least 10 bp) or DNA-RNA heteroduplex (at least 15 bp), single nucleotide specificity can be realized by this method.

The detail operational process and sequence of nucleic acid used in the experiment was respectively shown in Fig. S7 and Table S1.

3.2. Characterization of Fe_3O_4@Ag and SERS tags

The characterization results of Fe_3O_4@Ag and SERS tags were indicated in Fig. 1. As shown in the high resolution TEM of Fe_3O_4 and Fe_3O_4@Ag (Fig. 1a and b), the dimensions of Fe_3O_4 was approximately 400 ± 5 nm, the Ag shell thickness was approximately 10 ± 3 nm. Fig. 1c was the EDS elemental mapping of the Fe_3O_4@Ag, Ag atoms (yellow) and Au atoms (green) were surround located in the surface of Fe atoms (red) core area which was consistent with the Fe_3O_4 core and Au seed-Ag shell. The UV–vis spectra and magnetic hysteresis curves of Fe_3O_4 and Fe_3O_4@Ag was shown in Fig. S1. The saturation magnetization value of Fe_3O_4 and Fe_3O_4@Ag MNPs is 80 and 50 emu g^{-1} respectively; therefore the Fe_3O_4@Ag MNPs retain major magnetic properties of the Fe_3O_4 core and also can be completely separated from the solution with 20 s when the magnetic field was applied. Fig. 1d and e showed the high resolution TEM of Au@Ag NPs. The dimensions of Au@Ag was approximately 35 ± 5 nm, the Ag shell thickness was approximately 6 ± 2 nm. Fig. 1f was the EDS elemental mapping of the Au@Ag, Ag atoms (green) was surround located in the surface of Au atoms core (dark blue) which was consistent with the Au core and Ag shell. The UV–vis spectra of the Au NP and Au@Ag NP was shown in Fig. 1g. Fig. 1h was the SERS spectra of Au@DTNB and Au@Ag@DTNB NPs. It indicated 2-fold magnification of the Raman intensity compared Au@Ag@DTNB with Au@DTNB. In the SERS tag, DTNB was used as Raman molecule because of its large Raman scattering cross-section, no fluorescence interference, and free carboxyl groups as modification sites. DTNB could produce strong and concise SERS peaks located at 1063, 1152, 1332, and 1556 cm^{-1}, which are assigned to the succinimidyl N–C–O stretch overlapping with aromatic ring modes, the C–H deformation modes, the symmetric nitro stretch mode, and the aromatic ring C–C stretching modes, respectively (Wang et al., 2011).

The main Raman peak at 1332 $cm^{-1}$was the strongest characteristic peak of DTNB thus was used for quantitative determination. We also detect the Powder X-ray diffraction (XRD) of the Fe_3O_4, Fe_3O_4@Ag and Fe_3O_4@Ag-SERS tags and the result was shown in Fig S2. The XRD pattern showed that for our Fe_3O_4@Ag microspheres, the typical XRD pattern and the intensity of diffraction peaks of the Fe_3O_4, Au seed, and Ag shell were fixed and consistent with previous paper (Wang et al., 2015a, 2015b). After the Au@Ag SERS tags attached on the Fe_3O_4@Ag MNPs, the Au and Ag content increased, thus XRD peaks of the Au and Ag became stronger. Therefore, the obvious intensity increase in XRD peaks of the Au and Ag suggested that Fe_3O_4@Ag-SERS tags assemblies were successfully formed. It should be noted that the characteristic peaks for Au and Ag were too close to distinguish (Shen et al., 2013,).

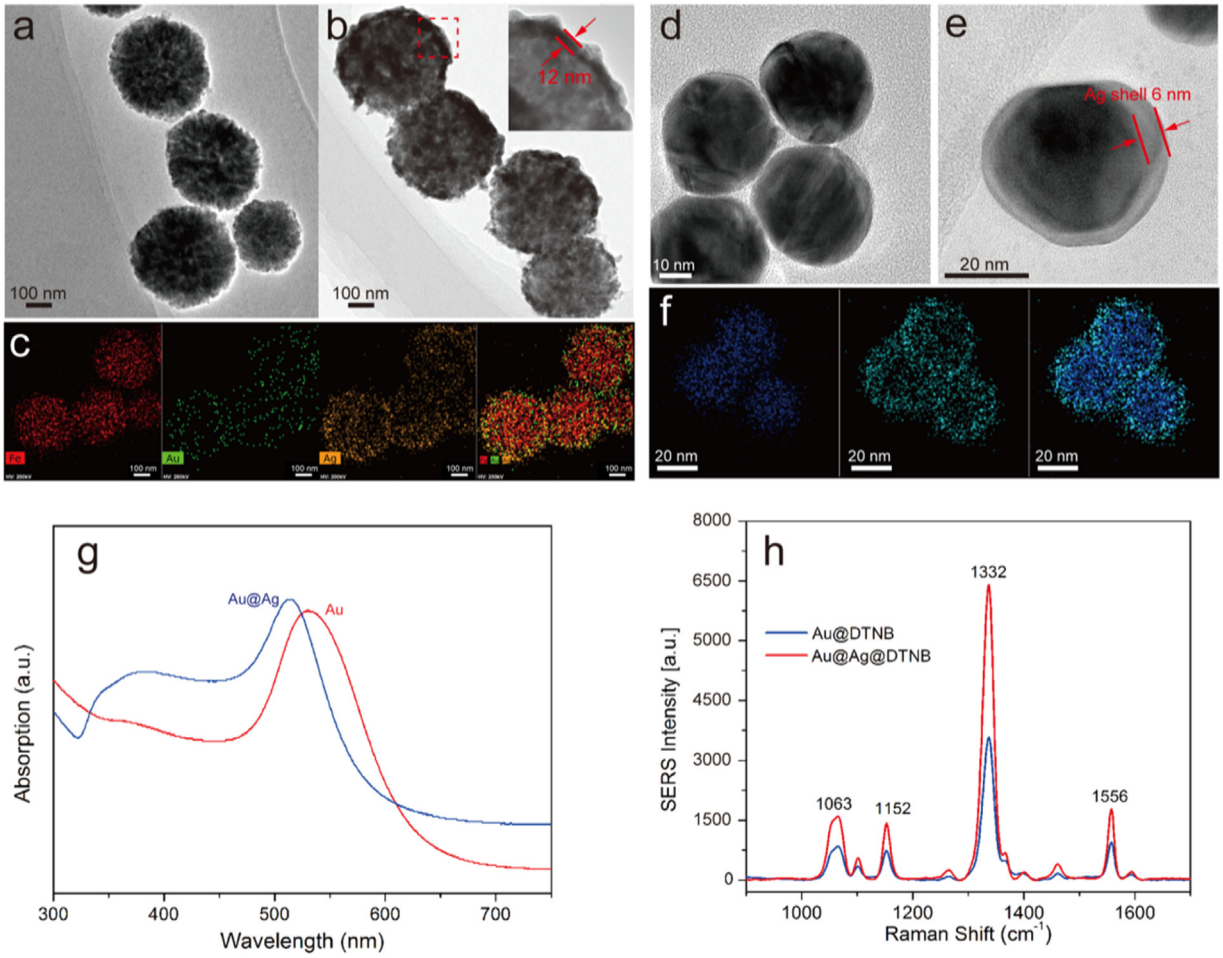

Fig. 1. (a) HRTEM images of the synthesized Fe_3O_4 and (b) the Fe_3O_4@Ag core-shell plasmonic nanoparticles; (c) Corresponding elemental mapping images of Fe_3O_4@Ag; (d-e) HRTEM images of the synthesized Au@Ag; (f) Corresponding elemental mapping images of Au@Ag (g) UV–visible spectra of the synthesized Au@Ag nanoparticles; (h) Raman intensity of Au@DTNB, Au@Ag@DTNB under the same conditions.

3.3. Characterization and principle verification of the SERS assay

Firstly, to ensure the modification of the DNA probes on the surface of Fe_3O_4@Ag, we detected the UV–visible spectra of the two terminal modified DNA supernatant before and after incubated with the carboxyl-Fe_3O_4@Ag and streptavidin-SERS tags respectively. As shown in Fig. S3, after centrifugation or magnetic separation, the UV–visible spectra of the residual supernatant decreased largely at 260 nm, which illustrated that the DNAs can both linked on the surface of Fe_3O_4@Ag through NH_2-COOH and on the surface of SERS tag through biotin-avidin interaction.

Further, the morphology character of the nanoparticles and reaction process were displayed by the SEM images. Fig. 2a and b were the SEM of the streptavidin-modified SERS tags and Fe_3O_4@Ag-DNA respectively. Fig. 2c was the product of Fe_3O_4@Ag-DNA incubated with streptavidin-modified SERS tags and magnetic separation. It can be found that SERS tags can conjunct on the surface of Fe_3O_4@Ag through the biotin-avidin interaction after magnetic separation. After adding target microRNAs and the DSN, the SERS tags can be dissociated from Fe_3O_4@Ag and then be washed away (Fig. 2d).

To verify the conjunction of Fe_3O_4@Ag and SERS tags further, the SERS signals of suspending streptavidin-modified SERS tags, Fe_3O_4@Ag-DNA before and after incubated with streptavidin-modified SERS tags(after magnetic concentration) was detected in the same other conditions. To simultaneously verify the detection principle, the SERS signals of Fe_3O_4@Ag-SERS tags assemblies with and without microRNA incubation was detected in the same other conditions and the result was shown in Fig. 2e-f. It can be seen that there was almost no signal for the Fe_3O_4@Ag-DNAs, the Fe_3O_4@Ag-SERS tags exhibited stronger SERS signal compared with Fe_3O_4-SERS tags (about 2-fold magnification) and suspending SERS tags (about 3-fold magnification), both because of the LSPR by the Ag shell of Fe_3O_4@Ag and more hot spots induced by the magnetic concentration. In the present of microRNA and DSN, obvious SERS attenuation can be found after reaction. It verified that the SERS intensity attenuation was in proportion to the microRNA.

As the Fe_3O_4@Ag-SERS tags core-satellite assemblies were the substrate for microRNA capture and DSN hydrolysis, the stability of the assemblies was very important. Here, the hydrodynamic sizes of the assembles were detected. Fig. 3a showed that the hydrodynamic sizes of the Fe_3O_4@Ag-DNA was about 428 ± 3 nm, after SERS tags conjunction, the hydrodynamic sizes of Fe_3O_4@Ag-SERS tags increased to 476 ± 5 nm (Fig. 3b). Here, we estimated the maximum average number of SERS tags around Fe_3O_4@Ag is statistically analyzed to be about 323 ± 5 by an approximate calculation, which was comparable with the previous reports with the similar assemble (Lu et al., 2016; Zhao et al., 2015a, 2015b). Fig. 3b and c showed the hydrodynamic sizes and the SERS intensity of the Fe_3O_4@Ag-SERS tags after storage at 4 °C for 90 days. It showed that the assemblies can provide steady hydrodynamic sizes and SERS signal with time lapses. Therefore, this SERS biosensor was stable enough for clinical diagnostic application.

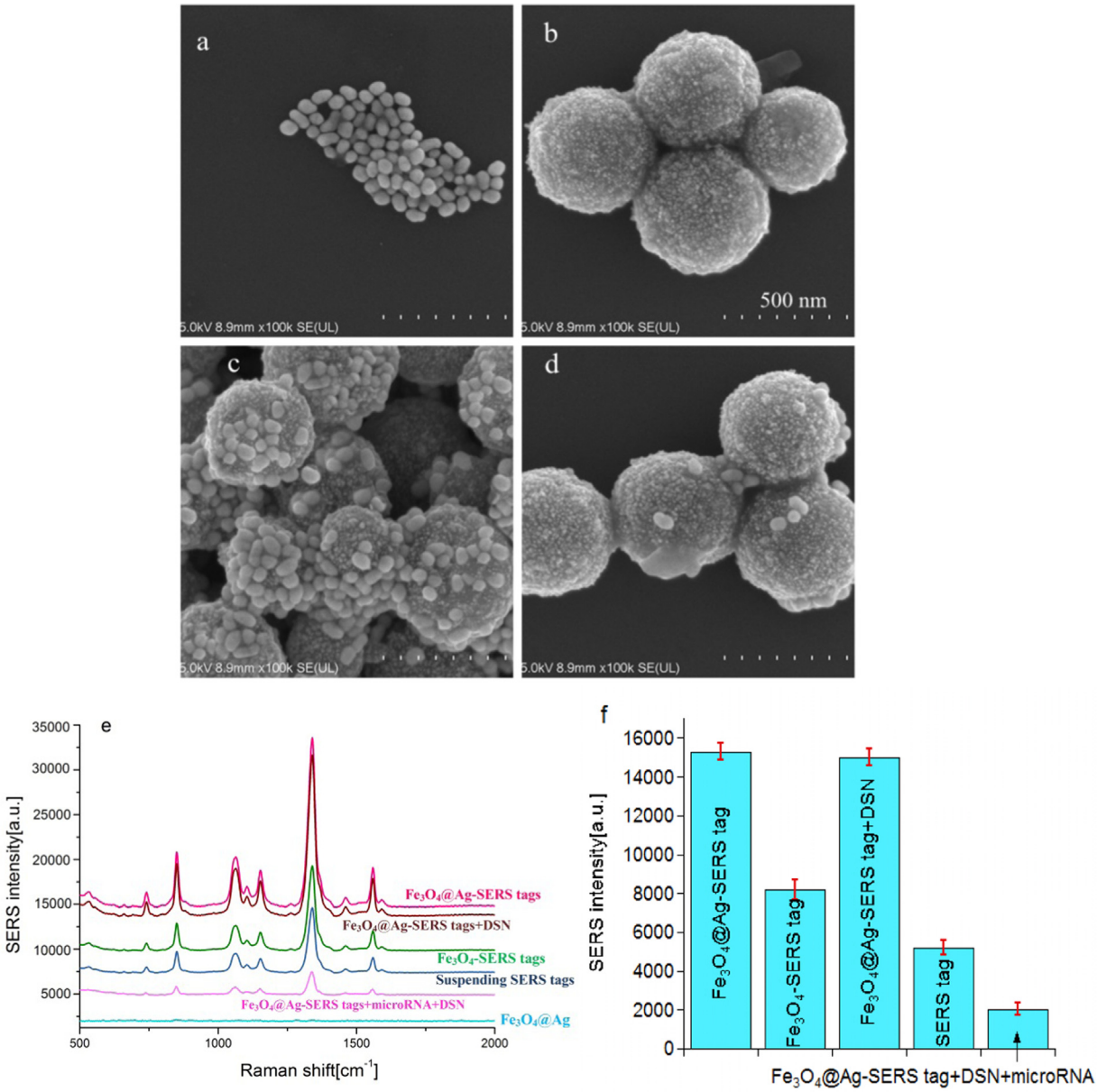

Fig. 2. SEM images of (a) SERS tags;(b) Fe_3O_4@Ag; (c) Fe_3O_4@Ag-SERS tags core-satellite assemblies; (d) Fe_3O_4@Ag-SERS tags in the presence of microRNA (10 pM) and DSN enzyme(0.25 units/μL);(e-f) SERS spectra and intensity of the different SERS systems. The error bars represent the standard deviation of three repetitive measurements of each sample.

3.4. Investigate the SERS enhancement factors and confirm the reproducibility of our SERS biosensor

It has been verified that the enormous enhancement of the SERS-active substrates was originated from both the physical (electromagnetic) mechanism and chemical mechanism. The physical mechanism plays a predominant role in Raman signal enhancement. Theoretically, the physical enhancement is proportionate to the fourth power of the EM field intensity. The "hot spots", which usually form at the tips or the gaps of the structure, are considered as the main factor that contributes to the physical enhancement. Herein, the hotspots were visualized using FDTD method as shown in Fig. 4a. The hotspots mainly located at the gaps between the Fe_3O_4@Ag particle and the Au@Ag NPs along the Y direction, because the plane wave source was Y polarized. The max EM field intensity ($|E/E_0|^2$) was calculated to be 829.207, which demonstrated that the enhancement originated from physical enhancement was about 6.87×10^5. Since the chemical mechanism normally provides about 10–100 folds enhancement, therefore, the enhancement factor of the whole biosensor was between the 10^6–10^7 (Wang et al., 2015a, 2015b). It should be noted that the model used here was not optimized, such as the gap between the Fe_3O_4@Ag particle and the Au@Ag NPs and the gap between the Au@Ag NPs. Thus, the EF would be much bigger in the practical SERS measurement.

To confirm the reproducibility of our method, we assessed detection of five SERS biosensors using 1 pM microRNA-10b in the same manner. For each biosensor, SERS signals were measured 3 times to get the standard deviation. As shown in Fig. 4b, the distribution of the Raman intensity (at 1332 cm^{-1}) revealed a low RSD of 3.03%. This result indicates that SERS intensity variation of five sensors is very low. Based on this experimental data, the SERS sensors are suitable for quantitative detection of microRNAs while ensuring consistent reproducibility.

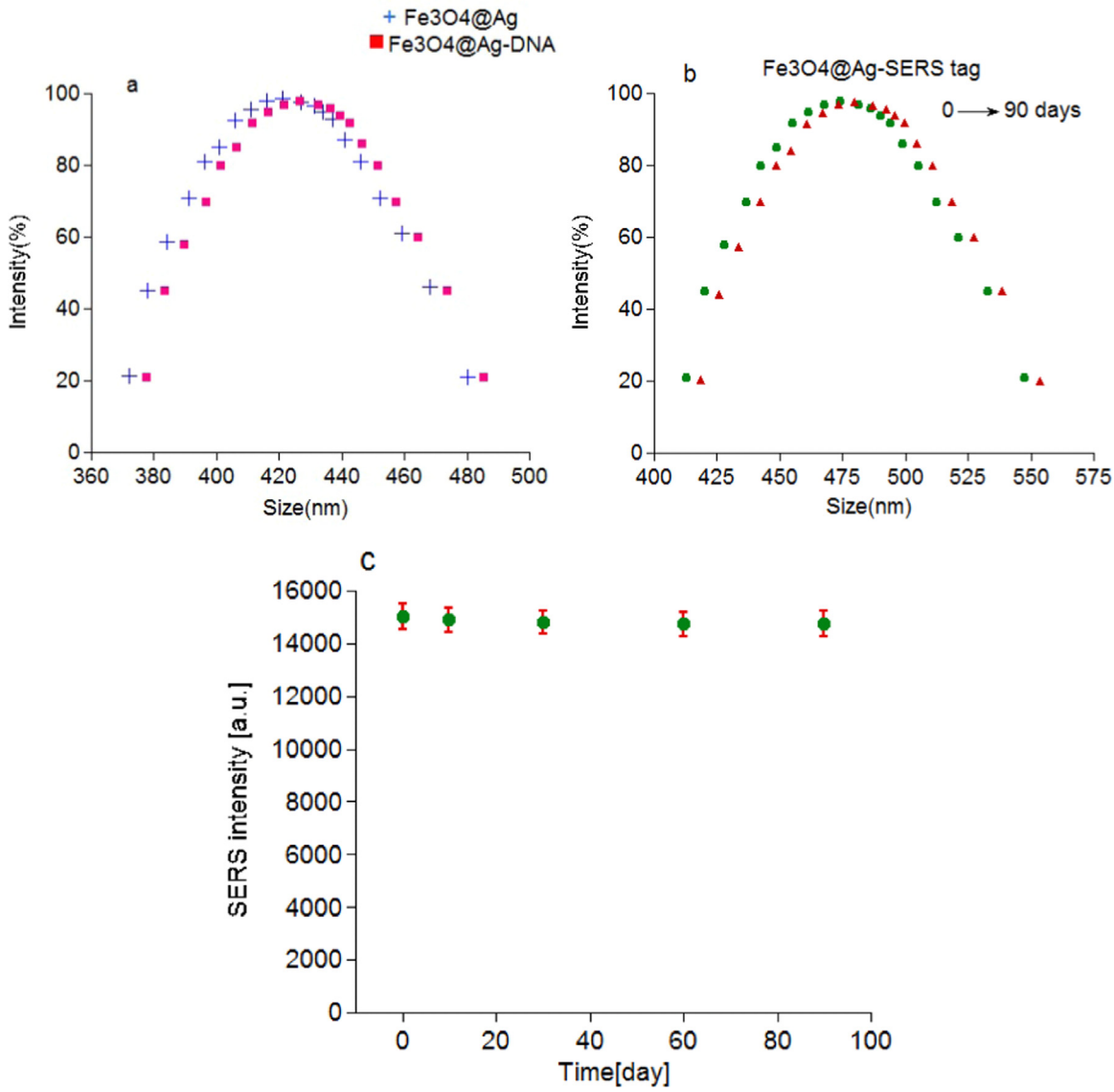

Fig. 3. (a) The hydrodynamic sizes of the Fe_3O_4@Ag and Fe_3O_4@Ag-DNA; (b-c) The hydrodynamic sizes and SERS intensity of the Fe_3O_4@Ag-SERS tags assemblies at 0 and 90 days storage. The error bars represent the standard deviation of three repetitive measurements of each sample.

3.5. Sensitivity and selectivity evaluation

Firstly, we optimize the experimental conditions for microRNA detection by SERS sensing. In order to improve the detection sensitivity, the concentration of DSN enzyme, the reaction temperature and reaction time were optimized with the presence of 1 pM of microRNA. As shown in Fig. S4a, the SERS intensity decrease with the temperature increasing from 30 to 45 °C, when higher than 45 °C, the SERS intensity begin to increase due to the inefficient hybridization between DNA and microRNA or reduced activity of DSN enzyme. Next, we evaluated the optimized concentration of DSN enzyme which is 0.25 U (Fig. S4b). For the optimization of reaction time, the value of SERS intensity decrease gradually with the prolonged reaction time and reaches a plateau after 50 min reaction (Fig. S4c). The saturated reaction indicates that no more SERS tags could be cleaved off from large MNPs after 50 min. Therefore, 45 °C was chosen as the reaction temperature, 0.25 U as the DSN enzyme concentration and 50 min as the reaction time for the following microRNA detection.

Under optimal conditions, the Raman spectra at different microRNA-10b concentrations had been detected and shown in Fig. 5. The SERS intensity of the nanocomposites after magnetic separation linear decreased with the concentration of microRNA-10b increasing from 2 aM to 100 pM. The detection limit was 1 a.M. by the three standard deviations of the noise principle, which was at least 100-fold lower than those of other methods using the SERS platform for microRNA detection (Qi et al., 2017; Yang et al., 2018; He et al., 2017; Wu et al., 2018; Zhou et al., 2017; Guo et al., 2018) and was comparable with the recent reported electrochemical microRNA sensors (Ghazizadeh et al., 2018). Moreover, we compared some recently reports for exosomal microRNA detection with this work in Table S3.

The specificity was assessed by control experiments for target microRNA-10b (1 fM), single-base mismatch microRNA-10a (1 pM) and the mixture of the two. As shown in Fig. 5c, there was observably SERS intensity decreasing in the presence of target microRNA-10b and the mixture, but for the microRNA-10a only, there was almost no change. These results demonstrated that with the help of DSN enzyme, target microRNA-10b can be recognized with the coexist of thousand-fold similar microRNAs.

To investigate the medium effects, we also evaluate the LOD value of microRNA-10b in health human plasma under the same other conditions with that in PBS buffer. As shown in Fig. S5a, a good linear response from 3 aM to 100 pM is observed, with the LOD of 1.8 aM (R^2

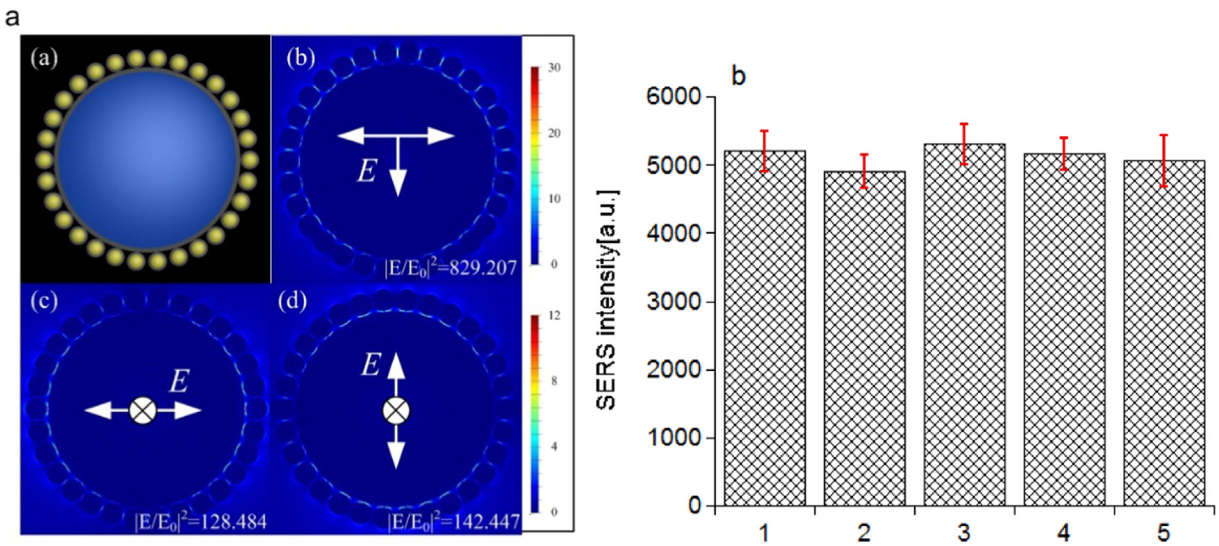

Fig. 4. (a) The simulation model and the EM distributions of three different conditions; (b) Average distribution of SERS intensities (at 1332 cm^{-1}) for five SERS sensors. The incident light had a wavelength of 785 nm. The error bars represent the standard deviation of three repetitive measurements of each sample.

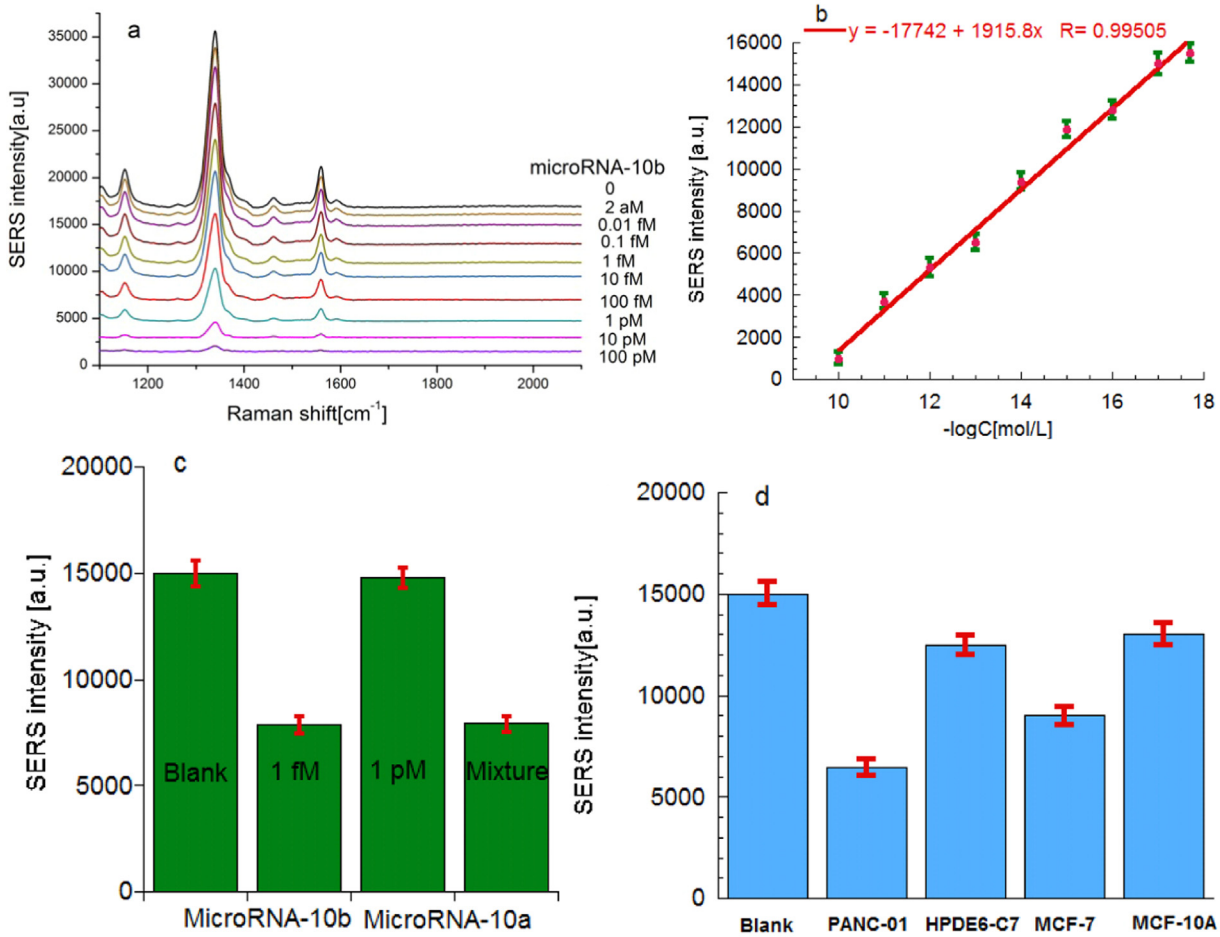

Fig. 5. (a) The SERS spectra of Fe_3O_4@Ag-SERS tags assemblies in the presence of different target microRNA10b concentrations; (b) The correlation analysis of SERS intensity (at 1332 cm^{-1}) and the negative logarithm of target microRNA10b concentration from 2 aM to 100 pM; (c) Specificity evaluated by microRNA-10b (1 fM), microRNA-10a (1 pM) and the mixture of the two samples(1 fM: 1 pM); (d) SERS intensity changes of the exosomal RNA samples extracted from the different cell lines. Blank represents SERS intensity of Fe_3O_4@Ag-SERS tags assemblies without any reagent after magnetic aggregation. The error bars represent the standard deviation of three repetitive measurements of each sample.

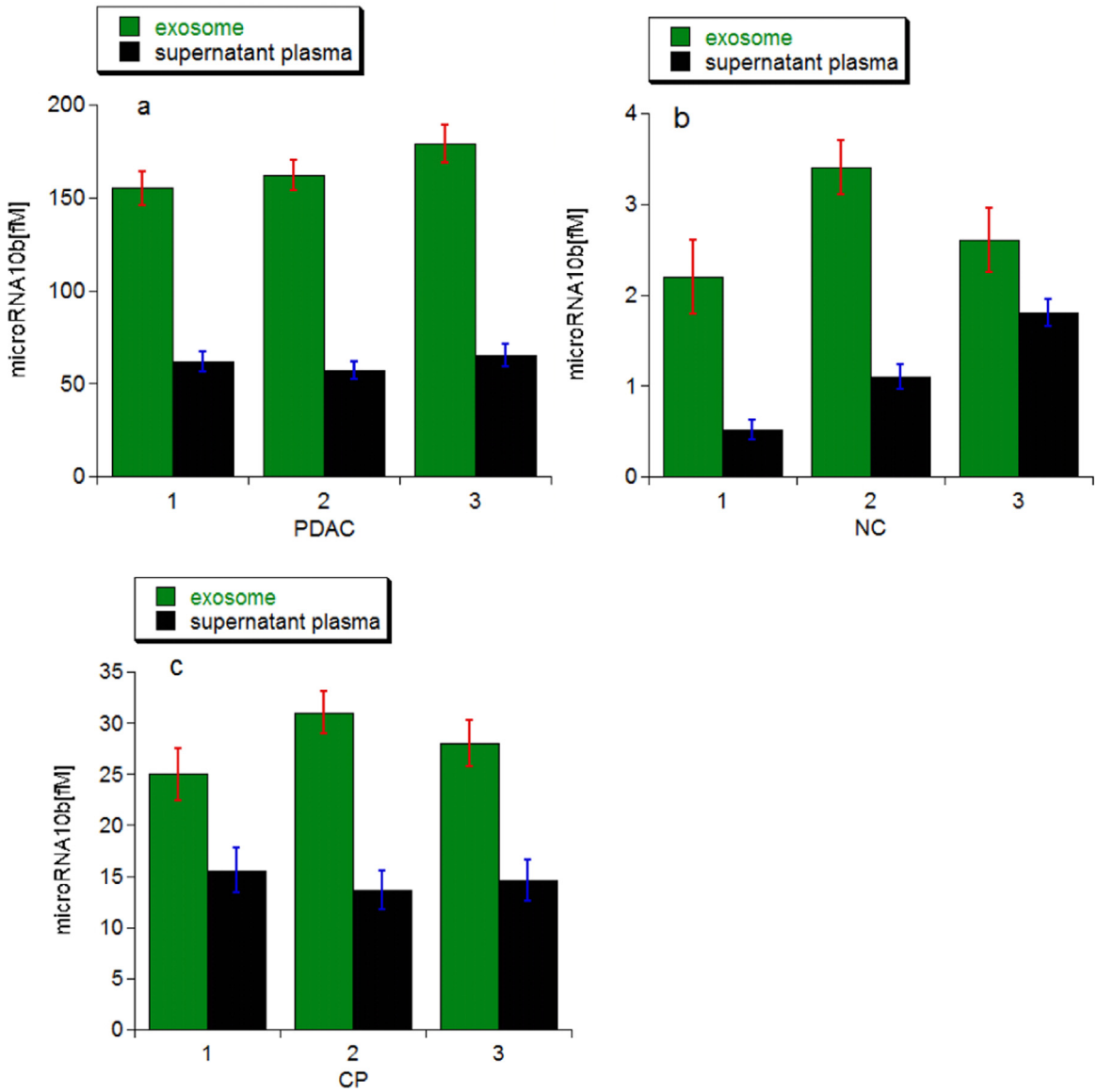

Fig. 6. Determination of microRNA-10b concentration in exosome and residual supernatant plasma from (a) three patients with PDAC, (b) three normal control (NC), and (c) three patients with CP using our SERS sensors. Exosome was collected from plasma samples and total RNA was extracted for microRNA detection; the residual supernatant plasma after exosome extracted of the serum was used for microRNA detection. The error bars represent the standard deviation of three repetitive measurements of each sample.

= 0.997). We also investigate the percent recovery by spiking a certain amount of microRNA-10b (10 fM, 1 pM, and 100 pM) into the same plasma to detect the SERS intensity after reaction. Based on the linear response, the percent recoveries can be obtained as 105.4%, 99.1% and 101.5% as shown in Fig. S5b. Therefore, the medium effect of human plasma is negligible. The slight differences in assay sensitivity between PBS buffer and human plasma may be induced by the differences in ionic strength or salt concentrations between PBS buffer and plasma and some coincidental non-specific adsorption of plasma protein on the surface of the SERS tags (Joshi et al., 2015).

The exosomes were collected from the culture medium of PANC-01, HPDE6-C7, MCF-10A and MCF-7, the total RNA was extracted respectively for microRNA-10b detection. The SERS intensity (at 1332 cm^{-1}) of the exosomal microRNA-10b from the 4 kinds of cell lines samples was shown in Fig. 5d, we found that the SERS intensity of the PANC-01 and MCF-7 samples were much lower than that of HPDE6-C7 and MCF-10A respectively, which proves the high levels of microRNA-10b in the cancer cell lines and can be used as cancer biomarkers (Ma et al., 2007; Sempere et al., 2010). Moreover, exosomes released into cell culture medium were purified and analyzed for protein expression and morphology (Fig. S6). We confirmed the exosomes for containing tetraspanins (e.g. CD9, CD63) and proteins involved in multivesicular biogenesis (β-actin), along with the negative control Calnexin (not found in exosomes) by western blotting analysis(Fig. S6a). Transmission electron microscopy showed that the purified exosomes had a round shape and proximate diameter of 120 nm (Fig. S6b), which are consistent with previously reported characteristics of exosomes (Liu et al., 2018).

3.6. Joint microRNA detection in exosome and residual supernatant plasma of clinic blood samples

The concentrations of microRNA-10b in different samples were determined and the result was shown in Fig. 6a-c. It showed that all three samples from PDAC patients (Fig. 6a) has higher microRNA-10b levels in both circulating exosomes and supernatant plasma compared with normal controls (Fig. 6b) and CP patients (Fig. 6c). The result revealed that microRNA-10b levels in exosomes from PDAC samples

were about 59-fold higher than samples of normal controls, 6-fold higher than samples of CP patients; the microRNA-10b levels in supernatant plasma from PDAC samples were about 63-fold higher than samples of normal controls, 4-fold higher than samples of CP patients; Table S2 provides the p-values for the statistical analysis based on diagnosis by comparison with normal values where indicated in Fig. 6. The result showed that the microRNA-10b showed significant differences between patients with PDAC, CP and normal control (NC) both in the exosome and supernatant plasma. Our result was consistent with the previous research (Joshi et al., 2015). Moreover, CP has been proved to be associated with a higher risk for developing PDAC and finding markers to show the risk of CP patients to develop PDAC will be meaningful (Lowenfels et al., 1993). In our observations, CP patients exhibit slight but significant increases in microRNA-10b levels in both the circulating exosomes and plasma compared with the normal controls. Therefore, real-time monitoring the rising of microRNA-10b levels in CP patients may help to pre-warning for patients that are at a high risk for developing PDAC.

To investigate the accuracy of our proposed method, the gold standard qRT-RCR (Cote et al., 2014) and our SERS biosensor were used in parallel to quantify the microRNA-10b levels of patients with PDAC, CP and normal controls. The concentration of microRNA-10b in exosomes collected from PDAC, CP and normal controls plasma samples was determined respectively. The result was shown in Fig. S8. Comparing our SERS and qRT-PCR based data, it can be seen that the microRNA-10b concentration is very consistent in the clinic samples, which conformed the reliability of our assay. Thus, our SERS-based assay also displays high accuracy and practical value in biological samples.

4. Conclusion

In conclusion, we present a SERS assay for one-step detection of microRNA in exosome and supernatant plasma of blood samples for diagnosing pancreatic cancer. Owing to the dual-SERS enhancement of the Fe_3O_4@Ag-SERS tags assemblies and the DSN-assisted recycling signal amplification, a detection limit of 1 aM with single-base mismatch recognition can be performed. Through the quantification of the microRNA-10b both in exosome and the residual supernatant plasma of blood samples from the patients, PDAC can be distinguished accurately from CP and normal controls. This SERS biosensor can quantify attomolar concentrations of microRNA biomarkers from biological samples by one-step and one-pot without extensive sample preparation, which can be expect for point-of-care clinical cancer diagnosis. In the future, we will focus on the multiple microRNAs detection to improve the detection efficiency.

CRediT authorship contribution statement

Yuanfeng Pang: Conceptualization, Methodology, Writing - original draft, Funding acquisition. **Chaoguang Wang:** Investigation, Software. **LuChun Lu:** Data curation. **Chongwen Wang:** Writing - review & editing. **Zhiwei Sun:** Supervision, Validation, Funding acquisition. **Rui Xiao:** Supervision, Validation, Funding acquisition.

Acknowledgements

This work was supported by the financial support through the National Natural Science Foundation of China (81702106 and 51605486) and the Infectious Diseases Major Project (2018ZX10712001-010).

Declaration of interests

None.

Appendix A. Supplementary material

Supplementary data associated with this article can be found in the online version at doi:10.1016/j.bios.2019.01.039.

References

Boriachek, K., Umer, M., Islam, M.N., Gopalan, V., Lam, A.K., Nguyen, N.T., Shiddiky, M.J.A., 2018. Analyst 143, 1662–1669.
Cote, G.A., Gore, A.J., McElyea, S.D., Heathers, L.E., Xu, H., Sherman, S., Korc, M., 2014. Am. J. Gastroenterol. 109, 1942–1952.
Datta, J., Vollmer, C.M., 2014. South. Med. J. 107, 256–263.
Dong, H., Hao, K., Tian, Y., Jin, S., Lu, H., Zhou, S.F., Zhang, X., 2014. Biosens. Bioelectron. 53, 377–383.
Ellis, L., Benedetti, J., Rothenberg, M., Willett, C., Tempero, M., Lowy, A., et al., 2009. J. Clin. Oncol. 27, 5660–5669.
Fang, S., Lee, H.J., Wark, A.W., Corn, R.M., 2006. J. Am. Chem. Soc. 128, 14044–14046.
Ge, Z.l., Lin, M.H., Wang, P., Pei, H., Yan, J., Shi, J.Y., Huang, Q., He, D.N., Fan, C.H., Zuo, Xl, 2014. Anal. Chem. 86, 2124–2130.
Ghazizadeh, E., Naseri, Z., Jaafari, M., Forozandeh-Moghadam, M., Hosseinkhani, S., 2018. Biosens. Bioelectron. 113, 74–81.
Goonetilleke, K.S., Siriwardena, A.K., 2007. Eur. J. Surg. Oncol. 33, 266–270.
Guo, R.Y., Yin, F.F., Sun, Y.D., Mi, L., Shi, L., Tian, Z.J., Li, T., 2018. ACS Appl. Mater. Interfaces 10, 25770–25778.
He, Y., Yang, X., Yuan, R., Chai, Y., 2017. Anal. Chem. 89, 8538–8544.
Hidalgo, M., 2010. N. Engl. J. Med. 362, 1605–1617.
Iorio, M.V., Croce, C.M., 2009. J. Clin. Oncol. 27, 5848–5856.
Joshi, G.K., Deitz-McElyea, S., Liyanage, T., Lawrence, K., Mali, S., Sardar, R., Korc, M., 2015. ACS Nano 9, 11075–11089.
Kim, J., Bamlet, W.R., Oberg, A.L., Chaffee, K.G., Donahue, G., Cao, X.J., Chari, S., Garcia, B.A., Petersen, G.M., Zaret, K.S., 2017. Sci. Transl. Med. 9, 5583.
Lee, Y.S., Dutta, A., 2009. Annu. Rev. Pathol. 4, 199–227.
Li, M., Cushing, S.K., Zhang, J., Suri, S., Evans, R., Petros, W.P., Gibson, L.F., Ma, D., Liu, Y., Wu, N., 2013. ACS Nano 4967–4976.
Liu, C.C., Xu, X.N., Li, B., Situ, B., Pan, W.L., Hu, Y., An, T.X., Yao, S.H., Zheng, L., 2018. Nano Lett. 18, 4226–4232.
Lowenfels, A.B., Maisonneuve, P., Cavallini, G., Ammann, R.W., Lankisch, P.G., Andersen, J.R., Dimagno, E.P., Andren-Sandberg, A., Domellof, L., 1993. N. Engl. J. Med. 328, 1433–1437.
Lu, W., Chen, Y.P., Liu, Z., Tang, W.B., Feng, Q., Sun, J., Jiang, X.Y., 2016. ACS Nano 10, 6685–6692.
Ma, D.D., Huang, C.X., Zheng, J., Tang, J.R., Li, J.S., Yang, J.F., Yang, R.H., 2018. Biosens. Bioelectron. 101, 167–173.
Ma, L., Teruya-Feldstein, J., Weinberg, R.A., et al., 2007. Nature 449, 682–688.
Pang, Y.F., Wang, C.W., Wang, J., Sun, Z.W., Xiao, R., Wang, S.Q., 2016. Biosens. Bioelectron. 79, 574–580.
Qavi, A.J., Kindt, J.T., Bailey, R.C., 2010. Anal. Bioanal. Chem. 398, 2535–2549.
Qi, L., Xiao, M.S., Wang, X.W., Wang, C., Wang, L.H., Song, S.P., Qu, X.M., Li, L., Shi, J.Y., Pei, H., 2017. Anal. Chem. 89, 9850–9856.
Qu, X.M., Xiao, M.S., Li, F., Lai, W., Li, L., Zhou, Y., Lin, C.L., Li, Q., Ge, Z.L., Wen, Y.L., Pei, H., Liu, G., 2018. ACS Appl. Bio Mater. 1, 859–864.
Qu, X.M., Zhu, D., Yao, Gb, Su, S., Chao, J., Liu, H.J., Zuo, X.L., Wang, L.H., Shi, J.Y., Wang, L.H., Huang, W., Pei, H., Fan, C.H., 2017. Angew. Chem. Int. Ed. 56, 1–5.
Sempere, L.F., Preis, M., Yezefski, T., Ouyang, H., Suriawinata, A.A., Silahtaroglu, A., Conejo-Garcia, J.R., Kauppinen, S., Wells, W., Korc, M., 2010. Clin. Cancer Res. 16, 4246–4255.
Shen, J.H., Zhu, Y.H., Yang, X.L., Zong, J., Li, C.Z., 2013. Langmuir 29, 690–695.
Siegel, R.L., Miller, K.D., Jemal, A., 2016. CA Cancer J. Clin. 66, 7–30.
Thind, A., Wilson, Extracell, C.J., 2016. Vesicles 5, 31292–31303.
Wang, C.H., Li, P., Wang, J.F., Rong, Z., Pang, Y.F., Xu, J.W., Dong, P.T., Xiao, R., Wang, S.Q., 2015a. Nanoscale 7, 18694–18707.
Wang, J.F., Wu, X., Wang, C.H., Shao, N., Dong, P.T., Xiao, R., Wang, S.Q., 2015b. ACS Appl. Mater. Interfaces 7, 20919–20929.
Wang, Z.Y., Zong, S.F., Chen, H., Wu, H., Cui, Y.P., 2011. Talanta 86, 170–177.
Wittmann, J., Jäck, H.M., 2010. Biochim. Biophys. Acta Rev. Cancer 1806, 200–207.
Wu, Y., He, Y., Yang, X., Yuan, R., Chai, Y.Q., 2018. Sens Actuators B Chem. 275, 260–266.
Xiao, M.S., Man, T.T., Zhu, C.F., Pei, H., Shi, J.Y., Li, L., Qu, X.M., Shen, X.Z., Li, J., 2018. ACS Appl. Mater. Interfaces 10, 7852–7858.
Yang, X., Wang, S.F., Wang, Y., He, Y., Chai, Y.Q., Yuan, R., 2018. ACS Appl. Mater. Interfaces 10, 12491–12496.
Yang, Y., Huang, J., Yang, X., Quan, K., Wang, H., Ying, L., Xie, N., Ou, M., Wang, K., 2015. J. Am. Chem. Soc. 137, 8340–8343.
Yin, B., Liu, Y., Ye, B., 2012. J. Am. Chem. Soc. 34, 5064–5067.
Yoga, Y., Yasunaga, M., 2011. J. Gastrointest. Oncol. 2, 215–222.
Zhang, C., Wang, C., Xiao, R., Tang, L., Huang, J., Wu, D., Liu, S., Wang, Y., Zhang, D., Wang, S., Chen, X., 2018. J. Mater. Chem. B. 6, 3751–3761.
Zhao, Y., Yang, Y., Luo, Y., Yang, X., Li, M., Song, Q., 2015a. ACS Appl. Mater. Interfaces 7, 21780–21786.
Zeng, D.D., Wang, Z.H., Meng, Z.Q., Wang, P., San, L.L., Wang, W., Shen, J.W., Mi, X.Q., 2017. ACS Appl. Mater. Interfaces 9, 24118–24125.
Zhao, Y., Yang, Y., Luo, Y., Yang, X., Li, M., Song, Q., 2015b. ACS Appl. Mater. Interfaces 7, 21780–21786.
Zhou, W., Tian, Y.F., Yin, B.C., Ye, B.C., 2017. Anal. Chem. 89, 6120–6128.
Zhu, C., Yang, G., Li, H., Du, D., Lin, Y., 2015. Anal. Chem. 87, 230–249.